Anomalous lineshapes and aging effects in two-dimensional correlation spectroscopy

František Šanda[a)]
Faculty of Mathematics and Physics, Institute of Physics, Charles University, Ke Karlovu 5, Prague 121 16, Czech Republic

Shaul Mukamel[b)]
Department of Chemistry, University of California, Irvine, California 92697-2025, USA

(Received 9 March 2007; accepted 10 September 2007; published online 18 October 2007)

Multitime correlation functions provide useful probes for the ensembles of trajectories underlying the stochastic dynamics of complex systems. These can be obtained by measuring their optical response to sequences of ultrashort optical pulse. Using the continuous time random walk model for spectral diffusion, we analyze the signatures of anomalous relaxation in two-dimensional four wave mixing signals. Different models which share the same two point joint probability distribution show markedly different lineshapes and may be distinguished. Aging random walks corresponding to waiting time distributions with diverging first moment show dependence of 2D lineshapes on initial observation time, which persist for long times. © *2007 American Institute of Physics*. [DOI: 10.1063/1.2793786]

I. INTRODUCTION

Simple relaxation theories break down when the relaxation is nonexponential and assumes, for example, a stretched-exponential or an algebraic form. Such *anomalous relaxation* has been observed in numerous physical systems ranging from single molecules and quantum dot spectral diffusion in fluorescence blinking trajectories,[1–6] protein folding,[7,8] charge-carrier transport, geophysical processes, and in economics.[9–13] Stochastic dynamics can be fully described by ensembles of trajectories of collective variables.[14] Statistical analysis of stochastic trajectories results in a hierarchy of multipoint correlation functions which carry increasing levels of information. Two point correlation functions provide the simplest measure of fluctuations and the most common evidence for anomalous relaxation. They are the easiest to sample experimentally and to predict theoretically. However, they do not uniquely characterize the system. Many models can be constructed that have the same two point correlations but very different higher order correlation functions. Anomalous dynamics implies that many timescales are relevant. These may represent various dynamical variables or metastable configurations in polymers or glassy systems.[15–17] Treating all relevant variables explicitly is not always possible. Some calculations only include directly accessible variables (such as the transition frequency in spectral diffusion)[18] and use a master equation for their probability densities; all other variables are projected out and represented through memory functions. The long time memories characteristic of anomalous relaxation are not compatible with the ordinary Markovian approximation which assumes fast memory loss. The master equations derived in this case[19,20] are thus limited to two point correlation functions and do not carry enough information to describe the multipoint correlation and response functions.[21,22]

Several practical strategies may be employed toward the simulation of multipoint correlation functions. One option is to use Markovian master equations with a large number of collective variables. Another possibility is to assume harmonic (Gaussian) processes which are exactly solvable.[23,24] All information is then contained in the spectral density, which may be tailored to give long tailed correlations.[17,25] A different class of solvable models are continuous time random walks (CTRWs),[26,27] which assume the erasure of all memory (renewal) when the relevant dynamical variables are changed (jumps). They portray the dynamics as a generalized random walk with a distributed waiting time or length for stochastic jumps between various states. Memory enters this model solely through the time t elapsed from last renewal time. Anomalous behavior is observed when the waiting time distribution function (WTDF) $\psi(t)$ for the next jump has long tails. We have recently proposed that lineshapes in coherent multidimensional optical spectroscopy may be used to probe anomalous multipoint correlation functions.[28] Algebraic singularities at transition frequencies and power-law cross-peak dynamics were predicted in the two-dimensional optical response of a two level chromophore to three laser pulses whose frequency undergoes a stochastic two state jump continuous time random walk with a power-law waiting time density function $\psi(t) \sim t^{-\alpha-1}$. In this paper we present more detailed simulations for this model and further demonstrate how it may be used to probe aging effects in systems that never equilibrate. Frequency domain signals such as linear absorption are ill defined in aging systems since they depend on the measurement time window. Two-dimensional correlation spectroscopy (2DCS) is a time-domain technique that uses ultrashort pulses. Such signals should provide unam-

[a)]Electronic mail: sanda@karlov.mff.cuni.cz
[b)]Electronic mail: smukamel@uci.edu

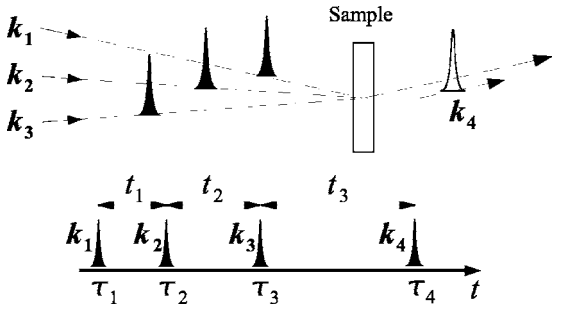

FIG. 1. Pulse configuration and time variables for a four wave mixing experiment.

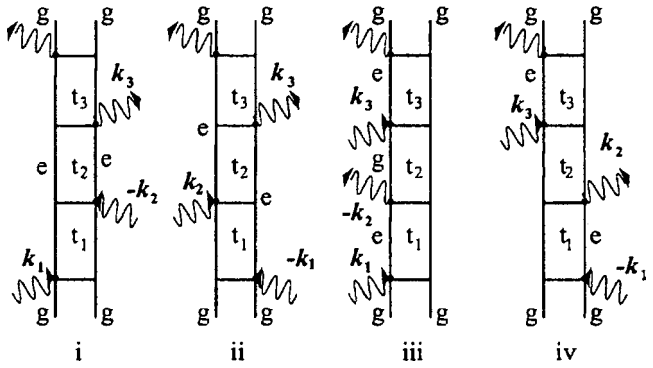

FIG. 2. Feynman diagrams for the third order response of a two level chromophore with wavevector $\mathbf{k_I}=-\mathbf{k_1}+\mathbf{k_2}+\mathbf{k_3}$ and $\mathbf{k_{II}}=\mathbf{k_1}-\mathbf{k_2}+\mathbf{k_3}$.

biguous signatures for aging, since all delay times are fully controlled. Different models may be distinguished by higher order nonlinear techniques.

We shall focus on two classes of WTDF which lead to anomalous spectral lineshapes. We assume asymptotic algebraic decay $\psi(t)\sim t^{-\alpha-1}$ which shows significant deviations from normal relaxation for $0<\alpha<2$.[29–32] For $1<\alpha<2$ stationary ensembles may be described by a proper choice of initial condition, which implies a special WTDF for the first jump $\psi'(t)$ which represents how the system was prepared. The anomalous multipoint correlations observed in fluorescence traces of conformation dynamics of flavin proteins[25] showed symmetries due to microscopic reversibility typical for stationary processes.

For $0<\alpha<1$, stationary ensembles cannot be constructed. System properties necessarily depend on the time elapsed from the initial preparation even when it is very long. This phenomenon is known as aging. Such random walks show fractal behavior related to Levy stable distributions, which generalize the Gaussian distributions of ordinary diffusion.[29] This case is fundamentally more complicated than $1<\alpha<2$: such random walks are nonergodic,[33] their time and ensemble averages may differ,[34] and special sample preparation for each run of the experiment is needed. Signatures of aging were observed in fluorescence blinking of single CdSe quantum dots, with $\alpha\approx 0.5$.[4,5,35] This is in agreement with the Sparre-Andersen theorem[36–38] which states that the first passage time of random walk with any symmetric distribution of jump lengths (including Levy flights) has a universal asymptotic $\sim t^{-3/2}$ decay. The origin of these long tailed WTDF is not fully understood.

Environment dynamics affects spectral lineshapes through modulations of the transition frequencies. However, extracting the fluctuation timescales from absorption lineshapes is not always possible and may require additional assumptions and the introduction of specific models. Nonlinear spectroscopies can distinguish between nonequivalent dynamical models whose linear response is identical. In 2DCS,[39–41] the system is subjected to 3 fs laser pulses (Fig. 1). The first pulse creates a coherence between the ground state and an excited state. Time evolution (free induction decay) during the first interval t_1 is related to the absorption lineshape by a Fourier transform. The second pulse erases the coherence, bringing the molecule to the ground or an excited state population. The transition frequency continues to change by interaction with the environment during the second interval t_2. Finally, a coherence is again created by the third pulse and detected during the third interval t_3. The various pathways for the density matrix of a two level chromophore in Liouville space are shown in Fig. 2. Correlations of the lineshapes during the first and the third interval provide information on environment dynamics during the intervening interval t_2. This supplements and greatly expands the information obtained from linear techniques.

2DCS can monitor dynamical processes at the femtosecond timescale; analogous 2D NMR techniques are commonly used to study much slower (millisecond) processes.[42] Two-dimensional infrared lineshapes have been used to probe the structure of peptides,[43] the picosecond hydrogen bonding dynamics by observing coherence transfer in molecular vibrations for phenol in benzene[44] and for acetonitrile in methanol.[45] In the visible, 2DCS techniques have been used to study exciton transfer in photosynthetic antennas.[46]

Simulations of 2DCS signals usually employ either Markovian or Gaussian models for spectral fluctuations. The response functions for Markovian fluctuations may be obtained by Green's function solution of the stochastic Liouville equations,[47–49] which combine a Markovian master equation for jump dynamics with the Liouville equation for coherent evolution. The response functions of a multilevel chromophore linearly coupled to harmonic bath (Gaussian fluctuations) may be obtained by the second order cumulant expansion using the Wick theorem. All higher response functions may then be factorized into products of two point quantities.

In the present work we extend our earlier work[28] to study signatures of aging in 2D lineshapes. In Sec. II we build a general CTRW multistate jump model and explain the condition of microscopic reversibility. The theory of 2D lineshapes is presented in Sec. III. In Sec. IV we discuss various parameter regimes of anomalous two state jump lineshapes. In Sec. V we study aging effects in 2CDS spectroscopy and compare two approaches to describe aging: CTRW and time-dependent Markovian master equation. The two models have same evolution of particle densities. The differences in 2DCS lineshape thus reflect the role of the underlying trajectory picture, i.e., unraveling of the master equation,[14] in multipoint probes.

II. TWO STATE CTRW JUMP MODEL: STATIONARITY, MICROSCOPIC REVERSIBILITY, AND AGING

In this section we briefly review the anomalous relaxation model used in Ref. 28. The multistate jump CTRW model is defined by a matrix $\hat{\Psi}(t)$ whose ij element is the WTDF for stochastic jumps from state j to state i. t is the time from the last jump where all memory is erased. The matrix is normalized as $\Sigma_i \int_0^\infty [\Psi]_{ij}(t)dt=1$.

In the simplest two state jump (TSJ) model,[48–51] bath has two states (a and b). We represent connection of density of renewals at various times in the a, b space by the matrix:

$$\hat{\Psi}(t)=\begin{pmatrix} 0 & \psi(t) \\ \psi(t) & 0 \end{pmatrix}. \tag{1}$$

The survival probability $\phi_i(t)$ (that no jump had occurred from state i for time t) defines the diagonal matrix of survival probabilities $[\hat{\Phi}_{ij}]=\delta_{ij}\phi_i$. It is connected to the waiting time density function $\psi(t)$ by $\phi_j(t)=\Sigma_i \int_t^\infty [\Psi]_{ij}(t')dt'$. The survival probability matrix thus connects the last renewal with final time

$$\hat{\Phi}(t)=\begin{pmatrix} \phi(t) & 0 \\ 0 & \phi(t) \end{pmatrix}. \tag{2}$$

The random walk is observed starting at time 0. The WTDF of the first jump $\psi'(t)$ may differ from $\psi(t)$ since it depends on how the system was prepared before $t=0$. Similarly, the $\hat{\Phi}'(t)$ matrix represents the survival probability for the first jump.

For a stationary process, the density of jumps to state i, η_i is connected to the total density to be in state i, ρ_i through

$$\rho_i=\rho_i(t)=\int_0^\infty \eta_i(t-t')\phi_i(t')dt'=\eta_i\int_0^\infty \phi_i(t)dt$$

$$=\eta_i\int_0^\infty t\sum_j [\Psi]_{ji}(t)dt=\eta_i\kappa_{1;i},$$

where we have used the fact that all densities ρ, η are time independent for stationary process and $\kappa_{1;i}\equiv\Sigma_j\int_0^\infty t[\Psi]_{ji}(t)dt$ is the mean waiting time in the ith state. It then follows that all $\kappa_{1;i}$ must be finite. The rate for the $j\to i$ jump is

$$\eta_j\int_0^\infty [\Psi]_{ij}(t)dt=\frac{\int_0^\infty [\Psi]_{ij}(t)dt}{\kappa_{1;j}}\rho_j.$$

We can now define the rate coefficients

$$A_{ij}\equiv\frac{\int_0^\infty [\Psi]_{ij}(t)dt}{\kappa_{1;j}} \quad \text{for } i\neq j,$$

$$A_{ii}=-\sum_{j;j\neq i} A_{ji}. \tag{3}$$

The stationary density ρ_j is thus obtained by the solution of the balance equation

$$\sum_j A_{ij}\rho_j=0.$$

Using the same arguments, the WTDF for the first jump is

$$[\Psi']_{ij}(t)=\frac{1}{\rho_j}\int_0^\infty [\Psi]_{ij}(t+t')\eta_j(-t')dt'$$

$$=\frac{\int_t^\infty [\hat{\Psi}]_{ij}(t')dt'}{\kappa_{1;j}}. \tag{4}$$

The stationary condition [Eq. (4)] is closely related to microscopic reversibility. CTRW is reversible if a trajectory i_1, $i_2,\ldots,i_n$ with waiting times $\xi_1,\xi_2,\ldots,\xi_n$ (last time is survival) is equally probable to its reverse $i_n,\ldots,i_1$ with waiting times $\xi_n,\ldots,\xi_1$. We thus require

$$\phi_{i_n}(\xi_n)[\hat{\Psi}]_{i_n i_{n-1}}(\xi_{n-1})\cdots[\hat{\Psi}]_{i_3 i_2}(\xi_2)[\hat{\Psi}']_{i_2 i_1}(\xi_1)\rho_{i_1}$$

$$=[\hat{\Psi}']_{i_{n-1} i_n}(\xi_n)[\hat{\Psi}]_{i_{n-2} i_{n-1}}(\xi_{n-1})\cdots[\hat{\Psi}]_{i_1 i_2}(\xi_2)\phi_{i_1}(\xi_1)\rho_{i_n} \tag{5}$$

for all paths (sequences and waiting times). Equation, (5) can only be satisfied provided (i) the time profile of WTDF is independent of jump direction $[\Psi]_{ij}(t)=T_{ij}\psi_j(t)$,[52,53] (ii) the rate coefficients for jump $A_{ij}=T_{ij}/\kappa_{1;j}$ $(i\neq j)$ must satisfy detailed balance[54]

$$\frac{T_{ij}\rho_j}{\kappa_{1;j}}=\frac{T_{ji}\rho_i}{\kappa_{1;i}},$$

and (iii) the probability of the first jump and the last survival are related through $\psi_i'(t)=\phi_i(t)/\kappa_{1;i}$ which recovers Eq. (4). Equation, (4) thus expresses microscopic reversibility of a stationary ensemble: the survival probability coincides with the probability for the first jump backward.

For the symmetric TSJ considered here [Eq. (1)] we simply have

$$\psi'(t)=\frac{\int_t^\infty \psi(t')dt'}{\kappa_1}=\frac{\phi(t)}{\kappa_1} \tag{6}$$

and symmetric densities $\rho_a=\rho_b=1/2$.

For $0<\alpha<1$, κ_1 diverges, and it is impossible to construct a stationary ensemble. Asymptotically the jump rate decreases to $1/\kappa_1$ which is 0 in this case.[31,55,56] This scenario applies for arbitrary initial conditions. Many properties now depend on the initial observation time (aging). The normal diffusion constant for a Brownian particle moving on a lattice scales as $\sim 1/\kappa_1$ and its variance grows linearly with time (Einstein relation) $\langle \Delta x^2\rangle \sim t/\kappa_1$. When κ_1 diverges, the particle loses its mobility at long times, and its variance $\langle \Delta x^2\rangle$ growth grows sublinearly $\sim t^\alpha$ (anomalous diffusion). Another remarkable point is that the random walker survives at initial position for long times and ergodicity is broken. As a corollary, time averages obtained in single molecule measurements may be different from ensemble averages.[34]

The simplest way to describe aging is by assuming that all random walks start by a jump made at some time t_0 before the first laser pulse. The common choice $\psi'(t)=\psi(t)$ implies $t_0=0$. The dependence on the initial observation time requires a t_0-dependent WTDF $\psi'(t;t_0)$. The consistent choice of $\psi'(t;t_0)$ will be discussed in Sec. IV.

III. SPECTRAL DIFFUSION IN 2DCS SIGNALS

We consider a two level chromophore with a ground $|g\rangle$ and an excited state $|e\rangle$, transition frequency Ω_{eg}, and dipole moment μ_{eg} subjected to three short laser pulses with an electric field $E(t)$, and described by the Hamiltonian

$$H_S = |e\rangle[\Omega_{eg} + \delta\Omega_{eg}(t)]\langle e| - E(t)\mu_{eg}[|g\rangle\langle e| + |e\rangle\langle g|], \quad (7)$$

$\delta\Omega_{eg}(t)$ are stochastic frequency fluctuations caused by interaction with the environment and described by the CTRW dynamics. Observable quantities are obtained by averaging over all possible stochastic paths of $\delta\Omega_{eg}(t)$.[57]

We associate the frequency fluctuations with different bath states i, each inducing a transition frequency shift $\delta\Omega_i$. In TSJ the transition frequency assumes the values $\delta\Omega_{eg} = \Omega_0$ (state a) and $-\Omega_0$ (state b).

The response of our two level chromophore to three optical pulses is described by the third order response functions. The various contributions to the response function, known as Liouville space pathways (Fig. 2), are labeled ν.[58] During the intervals $t_j \equiv \tau_j - \tau_{j-1}$, between successive laser interactions the system's density matrix is in a given state $|\nu^{(j)}\rangle = |ee\rangle$, $|gg\rangle$, $|eg\rangle$, or $|ge\rangle$ with corresponding frequencies $\Omega_\nu^{(j)} = 0, 0, \Omega_{eg}$, and $-\Omega_{eg}$, respectively. The latter are modulated by the state of the bath. The Liouville operator describing the evolution in the bath state $|eg\rangle$; $\dot{\rho}_{eg} = \hat{L}_{eg}\rho_{eg}$ is given by the following matrix in the a, b space:

$$\hat{L}_{eg} = \begin{pmatrix} -i\Omega_0 & 0 \\ 0 & i\Omega_0 \end{pmatrix}, \quad (8)$$

where $\hat{L}_{ge} = -\hat{L}_{eg}$, and $\hat{L}_{ee} = \hat{L}_{gg} = 0$.

We next define the generating function ρ_ν by the equation of motion.

$$\frac{d\rho_\nu}{dt} = -i\delta\Omega_\nu(t)\rho_\nu \quad (9)$$

with initial condition $\rho_\nu(0) = 1$. Here $\delta\Omega_\nu(t) = \delta\Omega^{(j)}(t)$ for $t \in (\tau_{j-1}, \tau_j)$. The third order response function for the νth pathway is then given by $R_\nu^{(3)}(t_3, t_2, t_1) \equiv \langle \rho_\nu \rangle$, where $\langle\ \rangle$ implies averaging over the ensemble of bath paths. Coherent signals are generated only in specific phase-matching directions. Below we focus on the $\mathbf{k_I} = -\mathbf{k}_1 + \mathbf{k}_2 + \mathbf{k}_3$ and $\mathbf{k_{II}} = \mathbf{k}_1 - \mathbf{k}_2 + \mathbf{k}_3$ directions. In the rotating wave approximation these are represented by the four Liouville space pathways shown in Fig. 2.

The $\mathbf{k_I}$ (photon echo) signal is[58]

$$\mathcal{S}_{\mathrm{I}}(t_3, t_2, t_1) = \left(\frac{i}{\hbar}\right)^3 \mu_{eg}^4 e^{-i\Omega_{eg}(t_3 - t_1)}[R_{ii}(t_3, t_2, t_1) + R_{iv}(t_3, t_2, t_1)], \quad (10)$$

and the $\mathbf{k_{II}}$ signal is

$$\mathcal{S}_{\mathrm{II}}(t_3, t_2, t_1) = \left(\frac{i}{\hbar}\right)^3 \mu_{eg}^4 e^{-i\Omega_{eg}(t_1 + t_3)}[R_i(t_3, t_2, t_1) + R_{iii}(t_3, t_2, t_1)]. \quad (11)$$

For stochastic models such as considered here the bath evolution and equilibrium state are independent of the state of the system ρ_{ee} or ρ_{gg} so that $R_i = R_{iii}$, $R_{ii} = R_{iv}$.

The third order correlation function for the νth pathway may be obtained by solving Eq. (9),

$$R_\nu^{(3)}(t_3, t_2, t_1) \equiv \theta(t_3)\theta(t_2)\theta(t_1) \times \left\langle \exp\left[-i\int_{\tau_2}^{\tau_3} \delta\Omega_{eg}(\tau_3')d\tau_3'\right] \times \exp\left[\mp i\int_{\tau_0}^{\tau_1} \delta\Omega_{eg}(\tau_1')d\tau_1'\right]\right\rangle, \quad (12)$$

where the upper sign represents $R_i = R_{iii}$ and the lower $R_{ii} = R_{iv}$.

The 2D signals are defined by frequency-frequency (ω_3, ω_1) correlation plots for a fixed t_2.

$$S_{\mathrm{I}}(\omega_3, t_2, \omega_1) \equiv -\mathrm{Im}\int\int \mathcal{S}_{\mathrm{I}}(t_3, t_2, t_1)e^{i(\omega_1 t_1 + \omega_3 t_3)}dt_1 dt_3, \quad (13)$$

$$S_{\mathrm{II}}(\omega_3, t_2, \omega_1) \equiv -\mathrm{Im}\int\int \mathcal{S}_{\mathrm{II}}(t_3, t_2, t_1)e^{i(\omega_1 t_1 + \omega_3 t_3)}dt_1 dt_3. \quad (14)$$

We shall also display the following combination, which shows simpler lineshapes with purely absorptive peaks:[59,60]

$$S_A(\omega_3, t_2, \omega_1) \equiv S_{\mathrm{I}}(\omega_3, t_2, -\omega_1) + S_{\mathrm{II}}(\omega_3, t_2, \omega_1). \quad (15)$$

The response is represented in a, b space by a matrix $\hat{G}^\nu$ whose jl element accounts for the contribution to $R_\nu^{(3)}$ from paths with an initial bath state l and final state j.

$$R_\nu^{(3)}(t_3, t_2, t_1) = \sum_{jl} [G^\nu]_{jl}(t_3, t_2, t_1)[\rho_\nu]_l(t = 0). \quad (16)$$

For Markovian relaxation $[\Psi]_{ij}(t) = T_{ij}e^{-t/\kappa_{1;j}}/\kappa_{1;j}$ each $\hat{G}^\nu$ may be factorized into a product of three Green's functions representing the time evolution during the t_1, t_2, and t_3 intervals whereby the density matrix is in the $\nu^{(1)}$, $\nu^{(2)}$, and $\nu^{(3)}$ states.

$$\hat{G}^\nu(t_3, t_2, t_1) = \hat{G}^{\nu^{(3)}}(t_3)\hat{G}^{\nu^{(2)}}(t_2)\hat{G}^{\nu^{(1)}}(t_1). \quad (17)$$

Green's functions can be calculated by solving the stochastic Liouville equations (SLEs).[47]

$$\frac{d\rho_\nu(t)}{dt} = (\hat{L} + \hat{A})\rho_\nu(t),$$

where $\hat{A}$ is the matrix of jump rate coefficients [Eq. (3)]. The SLE has recently been applied to describe vibrational 2D signals for frequency fluctuations modulated by hydrogen bonding of phenol in benzene,[61] conformation changes of peptides,[62] and infrared lineshapes of water.[63]

The simulation of systems with long memory is much more complex. Various types of reduced equations of motion for the CTRW dynamics have been developed[19,20] for calculating the two point correlation functions. These, however, may not be extended to multipoint quantities required for the description of 2DCS,[64] since the factorization, Eq. (17), does not hold for non-Markovian relaxation.

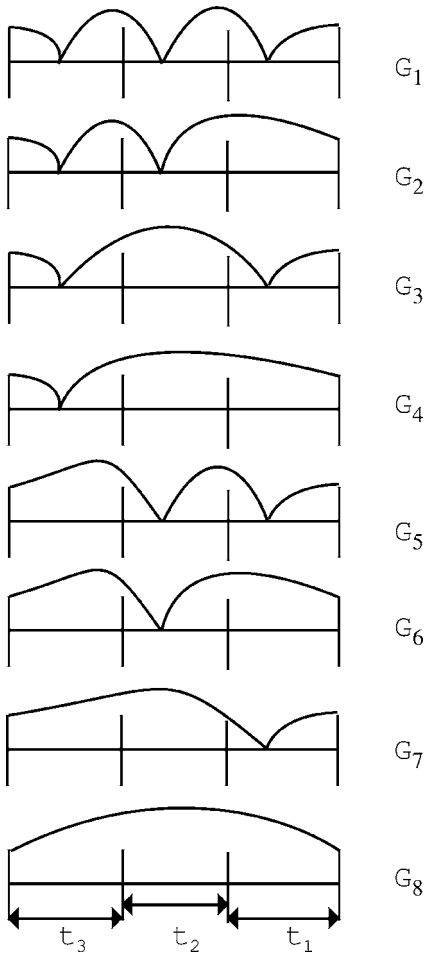

FIG. 3. The eight contributions to Green's function [Eq. (18)] of the third order response. Contributions represent paths with (when the line touch the axis) or without (when the line does not touch the axis) some jump during each of the three time intervals t_1, t_2, t_3.

We have recently[64] developed an algorithm for solving this model. This is based on the successive recurrent construction of a hierarchy of Green's functions. It relies on the renewal property computing the CTRW.[57] Below we present an alternative, more intuitive, derivation which is reminiscent of Green's function method.

We need to maintain a bookkeeping of whether or not there was a jump during each of the three time intervals t_1, t_2, t_3. For each of the three intervals we must distinguish between two possibilities, either there was no jump or there was a least one jump. $\hat{G}^{\nu}$ is thus given by a sum of $2^3=8$ terms each representing one type of path in bath space.

$$\hat{G}^{\nu}(t_3,t_2,t_1)=\sum_{m=1}^{8}\hat{G}_m^{\nu}(t_3,t_2,t_1). \tag{18}$$

These terms are depicted in Fig. 3, where the presence of any ($\geqslant 1$) jump in a given time interval is represented by the trajectory touching the time axis.

$\hat{G}_m^{\nu}$ are conveniently recast in Laplace space. We define (our notation is similar to Ref. 65)

$$\hat{\tilde{\Psi}}(s-\hat{L})\equiv\int_0^{\infty}e^{-st}\hat{\Psi}(t)\exp(\hat{L}t)dt.$$

This implies for our TSJ model

$$\hat{\tilde{\Psi}}(s-\hat{L}_{eg})=\begin{pmatrix}0 & \tilde{\psi}(s-i\Omega_0)\\ \tilde{\psi}(s+i\Omega_0) & 0\end{pmatrix}, \tag{19}$$

where $\tilde{\psi}(s)\equiv\int_0^{\infty}\psi(t)e^{-st}dt$ is the Laplace transform of ψ. $\hat{\tilde{\Phi}}(s-\hat{L})$ for the survival function is defined similarly

$$\hat{\tilde{\Phi}}(s-\hat{L}_{eg})=\begin{pmatrix}\tilde{\phi}(s+i\Omega_0) & 0\\ 0 & \tilde{\phi}(s-i\Omega_0)\end{pmatrix}. \tag{20}$$

$\hat{G}_m^{\nu}$ is expressed as a matrix product of the propagators through the intervals with any jump in the particular interval (if the trajectory touches the axis in Fig. 3), with additional factors for segments connecting different intervals. These ensure that the bath state does not change between the last jump in the earlier interval and the first jump in the later interval. Both factors will be described below.

We first calculate the evolution for a fixed state of bath where no jump occurs over several time intervals. Let us assume that the state is fixed for time $t_{m'}$ in the mth interval, until time $t_{l'}$ in some subsequent lth interval and during all the intermediate intervals t_i, $l>i>m$. The probability of this evolution is either $\hat{\Psi}$, $\hat{\Psi}'$, $\hat{\Phi}$, or $\hat{\Phi}'$ depending on the path. The propagator connecting the state immediately after t_m' and after t_l' is given by

$$\begin{aligned}\hat{\Upsilon}(\Psi,t_l',t_{l-1},\ldots,t_m')&=\hat{\Psi}\left(t_l'+t_m'+\sum_{i=m+1}^{l-1}t_i\right)\\&\times\exp\left(\hat{L}^{(l)}t_l'+\hat{L}^{(m)}t_m'+\sum_{i=m+1}^{l-1}\hat{L}^{(i)}t_i\right),\end{aligned} \tag{21}$$

where $\hat{L}^{(i)}=\pm\hat{L}_{eg},0$, depending on the state of the density matrix in the ith interval. This contribution may appear in several ways. Either for the evolution between the last jump in the mth interval and the successive jump, first in the lth interval, or for the very first jump when the t_m' interval does not exist and $\Psi\rightarrow\Psi'$. It also appears for the survival from the very last jump when t_l' disappear and $\Psi\rightarrow\Phi$. Finally, when no jump occurs, then $\Psi\rightarrow\Phi'$, t_l' is absent, and $t_m'=t_1$.

The second ingredient in our calculation is the propagator between first and last jump in the kth interval described by the integral equation

$$\hat{\Sigma}(\tau)=\int_0^{\tau}\hat{\Psi}(\tau-\tau')\exp[-i\hat{L}^{(k)}(\tau-\tau')]\hat{\Sigma}(\tau')d\tau', \tag{22}$$

with $\hat{\Sigma}(0)=\hat{1}$. The matrix Σ connects the arrival densities at two times within the same interval t_j. By solving Eq. (22) in Laplace space, we obtain the following propagator through the kth interval:

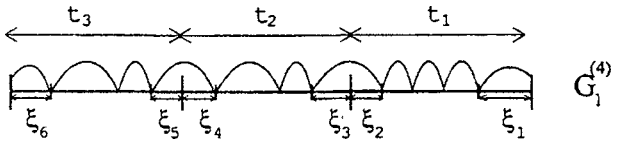

FIG. 4. Integration time variables in Eq. (24).

$$\hat{\Sigma}(s_k) \equiv [1 - \hat{\tilde{\Psi}}(s_k - \hat{L}^{(k)})]^{-1}. \tag{23}$$

This contribution appears provided some jump had occurred in the kth interval, (i.e., the trajectory touches the axis in the kth interval in Fig. 3.) Equation (23) can be interpreted as a summation of a geometric series for paths with 1,2, … jumps in Laplace space, where time convolutions become simple multiplications.

All of these factors should be convoluted in time to generate the trajectory. For instance, the domain of integration for the first contribution G_1^{ν} is shown in Fig. 4:

$$\begin{aligned}\hat{G}_1^{\nu}(t_3,t_2,t_1) &= \int_0^{t_3} d\xi_6 \int_0^{t_3-\xi_6} d\xi_5 \int_0^{t_2} d\xi_4 \int_0^{t_2-\xi_4} d\xi_3 \\ &\times \int_0^{t_1} d\xi_2 \int_0^{t_1-\xi_2} d\xi_1 \hat{\Upsilon}(\Phi,\xi_6)\hat{\Sigma}(t_3-\xi_6-\xi_5) \\ &\times \hat{\Upsilon}(\Psi,\xi_5,\xi_4)\hat{\Sigma}(t_2-\xi_4-\xi_3)\hat{\Upsilon}(\Psi,\xi_3,\xi_2) \\ &\times \hat{\Sigma}(t_1-\xi_2-\xi_1)\hat{\Upsilon}(\Psi',\xi_1).\end{aligned} \tag{24}$$

This results in a simple product in Laplace space

$$\begin{aligned}\hat{\tilde{G}}_m^{\nu}(s_3,s_2,s_1) &= \hat{\tilde{\Upsilon}}(\Phi,s_3)\hat{\tilde{\Sigma}}(s_3) \\ &\times \hat{\tilde{\Upsilon}}(\Psi,s_3,s_2)\hat{\tilde{\Sigma}}(s_2)\hat{\tilde{\Upsilon}}(\Psi,s_2,s_1)\hat{\tilde{\Sigma}}(s_1)\hat{\tilde{\Upsilon}}(\Psi',s_1).\end{aligned} \tag{25}$$

We have already calculated Laplace domain $\tilde{\Sigma}$ [Eq. (23)], Υ can be easily transformed as well, leading to equivalent results to those reported in Appendix C of Ref. 64. Equation (25) is finally expanded in terms of the matrices $\hat{\Phi}$, $\hat{\Psi}$ and the complete expressions agree with Appendix D of Ref. 64, where it was obtained in a different way.

Since the response functions [Eq. (12)] are causal, the 2D lineshapes [Eq. (14)] may be obtained by analytical continuation of s_1, s_3 (the Laplace variable conjugate to t_1 and t_3). The t_2 variable is obtained by reverse Laplace transform using Bromwich integral,

$$\begin{aligned}S_{\mathrm{I}}(\omega_3,t_2,-\omega_1) &= \frac{\mu_{eg}^4}{\pi\hbar^3}\,\mathrm{Im}\int_{-i\infty}^{i\infty} ds_2 e^{s_2 t_2} \\ &\times \tilde{R}_{ii}(s_3=-i(\omega_3-\Omega_{eg}),s_2,s_1=i(\omega_1-\Omega_{eg})),\end{aligned}$$

$$\begin{aligned}S_{\mathrm{II}}(\omega_3,t_2,\omega_1) &= \frac{\mu_{eg}^4}{\pi\hbar^3}\,\mathrm{Im}\int_{-i\infty}^{i\infty} ds_2 e^{s_2 t_2} \\ &\times \tilde{R}_i(s_3=-i(\omega_3-\Omega_{eg}),s_2,s_1=-i(\omega_1-\Omega_{eg})).\end{aligned}$$

For $t_2=0$ these integrals may be calculated analytically. The resulting two-interval functions may be alternatively obtained by directly building the two interval (t_3,t_1) response function.

IV. LINESHAPES FOR STATIONARY ANOMALOUS RANDOM WALKS

Microscopic reversibility in stationary ensembles implies that $\mathcal{S}_I(t_3,t_2,t_1)=-\mathcal{S}_I^*(t_1,t_2,t_3)$ which in the frequency domain gives

$$S_{\mathrm{I}}(\omega_3,t_2,-\omega_1) = S_{\mathrm{I}}(\omega_1,t_2,-\omega_3). \tag{26}$$

Similarly $\mathcal{S}_{\mathrm{II}}(t_3,t_2,t_1)=\mathcal{S}_{\mathrm{II}}(t_1,t_2,t_3)$ which implies

$$S_{\mathrm{II}}(\omega_3,t_2,\omega_1) = S_{\mathrm{II}}(\omega_1,t_2,\omega_3). \tag{27}$$

Combining Eqs. (26) and (27) with Eq. (15), we obtain the following symmetry of the lineshape:

$$S_A(\omega_3,t_2,\omega_1) = S_A(\omega_1,t_2,\omega_3). \tag{28}$$

Thus S_I, S_{II}, and S_A are symmetric to the interchange of ω_1 and ω_3.

When during the t_3 interval the bath has lost its memory of its state during t_1 (e.g., normal relaxation with $t_2\to\infty$), the response functions may be factorized as

$$\mathcal{S}_{\mathrm{I}}(t_3,t_2,t_1) = 2(i/\hbar)K(t_3)K^*(t_1) \tag{29}$$

and

$$\mathcal{S}_{\mathrm{II}}(t_3,t_2,t_1) = 2(i/\hbar)K(t_3)K(t_1). \tag{30}$$

Here

$$K(t) \equiv (i/\hbar)\mu_{eg}^2 e^{-i\Omega_{eg}t}\left\langle \exp\left[-i\int_0^t \delta\Omega_{eg}(\tau)d\tau\right]\right\rangle$$

is the linear response function for stationary ensembles. Its Fourier transform gives the absorption lineshape

$$W_A(\omega) \equiv \mathrm{Im}\int_0^{\infty} K(t)\exp[i\omega t]dt. \tag{31}$$

(The absorption of a nonstationary ensemble is not proportional to the Fourier transform of the linear response function.[50])

Using Eqs. (29)–(31), S_A then reduces to the product of the linear absorption lineshapes[66]

$$\hbar S_A(\omega_3,t_2\to\infty,\omega_1) = 4W_A(\omega_1)W_A(\omega_3). \tag{32}$$

Algebraic memory decays will result in a slow convergence to this asymptotic lineshape. In addition, as will be shown below, the spectra diverge at certain frequencies where the factorization [Eq. (32)] does not hold.

We shall consider a specific model of anomalous relaxation with the WTDF:[30,64]

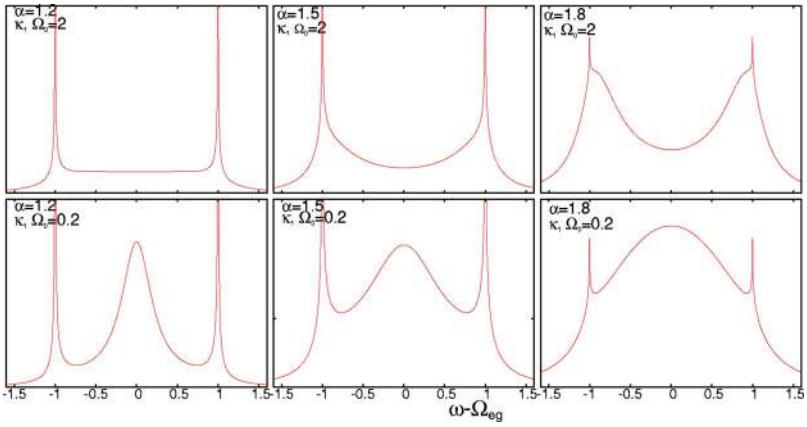

FIG. 5. (Color online) Linear absorption for slow $\kappa_1\Omega_0=2$ (top panel) and fast $\kappa_1\Omega_0=0.2$ fluctuations and different α as indicated. $\Omega_0\kappa_A=0.5$.

$$\tilde{\psi}(s)=\frac{1}{1+\kappa_1 s/[1+(\kappa_A s)^{\alpha-1}]},\quad 1<\alpha<2, \tag{33}$$

κ_1 is the mean of $\psi(t)$, while κ_A controls the long time algebraic tails $\psi_W(t)\sim\kappa_A^{\alpha-1}\kappa_1/t^{\alpha+1}$.

Note that Eq. (6) may be conveniently represented in Laplace space

$$\tilde{\psi}'(s)=\frac{1-\tilde{\psi}(s)}{s\kappa_1}.$$

We first consider the linear response obtained from one-interval Green's function

$$K(t)=\sum_{jl} Q_{jl}(t)\rho(0)_l.$$

The kernel may be calculated by

$$\hat{Q}(t)=\hat{\Upsilon}(\Phi',t)+\int_0^t d\xi_2\int_0^{t-\xi_2} d\xi_1\hat{\Upsilon}(\Phi,\xi_2)\times\hat{\Sigma}(t_1-\xi_2-\xi_1)\hat{\Upsilon}(\Psi',\xi_1).$$

Transforming into the Laplace space domain yields[50,64,65]

$$\hat{\tilde{Q}}(s)=\hat{\tilde{\Phi}}'(s-\hat{L})+\hat{\tilde{\Phi}}(s-\hat{L})[1-\hat{\tilde{\Psi}}(s-\hat{L})]^{-1}\hat{\tilde{\Psi}}'(s-\hat{L}). \tag{34}$$

Combining Eqs. (31), (33), and (34) we finally get

$$W(\omega+\Omega_{eg})=\frac{2\Omega_0^2}{(\Omega_0^2-\omega^2)^2}\mathrm{Re}\,\frac{1}{\kappa_1+\kappa_A^{\alpha-1}[(i\Omega_0-i\omega)^{\alpha-2}+(-i\omega-i\Omega_0)^{\alpha-2}]+i(\omega-\Omega_0)^{-1}+i(\omega+\Omega_0)^{-1}}. \tag{35}$$

In all plots we use dimensionless frequency units $(\omega_j-\Omega_{eg})/\Omega_0$ by setting $\Omega_{eg}=0$, $\Omega_0=1$. In Fig. 5 we display the absorption spectrum in the slow ($\kappa_1\Omega_0>1$, top) and the fast ($\kappa_1\Omega_0<1$, bottom) fluctuation limits. The lineshape has two peaks at $\omega=\pm1$ and in the fast fluctuation limit we obtain a finite central peak.[50,64] The fraction of particles that remained at the initial position is significant (not exponentially small) at all times. This results in the divergence of peaks at $\omega=\pm1$

$$W(\omega)\approx C|\Delta\omega|^{\alpha-2}, \tag{36}$$

with $C=\cos[\pi(1-\alpha/2)]\kappa_A^{\alpha-1}/2$, and where the detuning is $\Delta\omega\equiv\omega-\Omega_{eg}-\Omega_0$ for $\omega=1$ and $\Delta\omega\equiv\omega-\Omega_{eg}+\Omega_0$ for $\omega=-1$ peak.[50,64]

The parameter α controls the peak singularity. For $\alpha\to2$ the divergence is cured and we approach the Markovian lineshape. For fast fluctuations $\Omega_0\kappa_1\ll1$ the central peak grows, as κ_1 becomes shorter. This is reminiscent of the motional narrowing for the Markovian case. However, the two divergent peaks still retain an anomalous lineshape.

In Fig. 6(a) we display the $S_I(\omega_3,-\omega_1)$, $S_{II}(\omega_3,\omega_1)$, and $S_A(\omega_3,\omega_1)$ signals for slow fluctuations $\Omega_0\kappa_1\gg1$ and $t_2=0$. Similar to the Markovian case,[61] all panels show two diagonal peaks at $(\omega_3,\omega_1)=(1,1)$ and $(-1,-1)$. However, the peaks are non-Lorentzian and divergent. S_I and S_{II} diverge along the $\omega_1=\pm1$, $\omega_3=\pm1$ lines, but much of this divergence is canceled in S_A which only diverges at peaks (1,1) and $(-1,-1)$.

We next examine the analytic structure of these divergencies for the $\omega_1=1$ and $\omega_3=1$ lines. The slowest decay is connected with the survival function for the first jump $\phi'(t)\sim t^{1-\alpha}$. $\hat{G}_\nu^8$ is thus the most rapidly divergent term. The analysis of peak divergencies thus reduces to the $\hat{G}_\nu^8$ contribution. We denote $\Delta\omega_3\equiv\omega_3-\Omega_{eg}-\Omega_0$ and $\Delta\omega_1\equiv\omega_1-\Omega_{eg}-\Omega_0$ and find

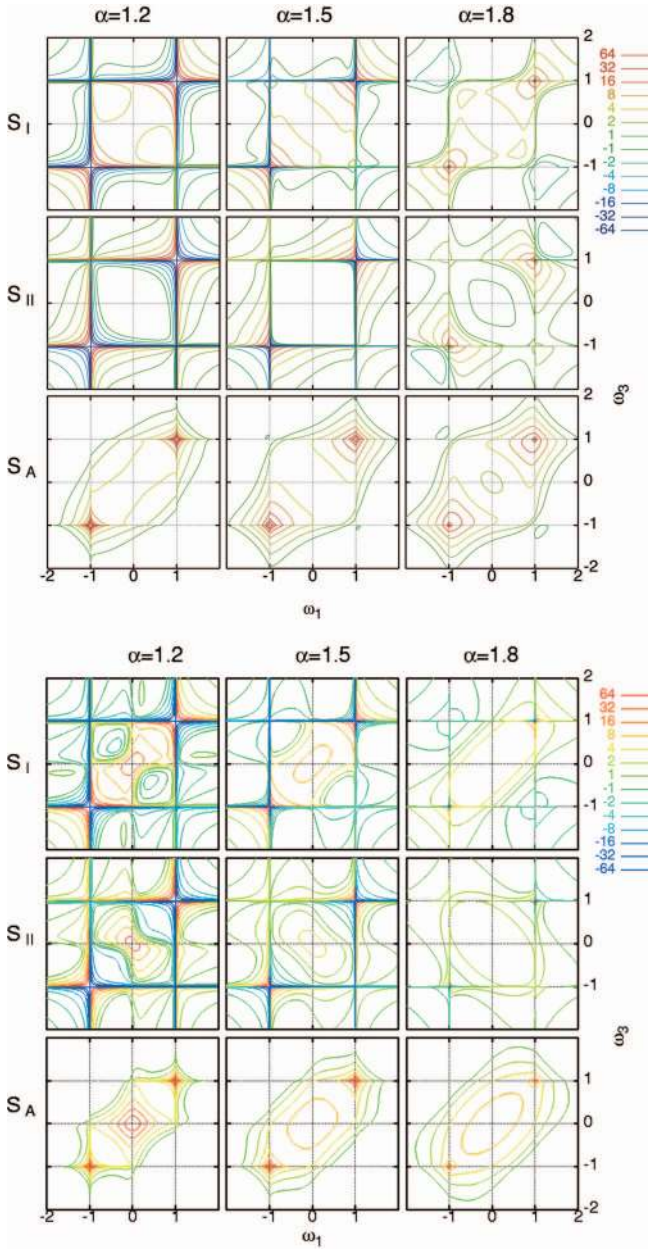

FIG. 6. (Color) (A) The $S_{\mathrm{I}}(\omega_3,0,-\omega_1)$ (top), $S_{\mathrm{II}}(\omega_3,0,\omega_1)$ (middle), and $S_A(\omega_3,0,\omega_1)$ (bottom) signals [Eq. (15)] for the WTDF [Eq. (33)] at $t_2=0$, for slow fluctuations $\Omega_0\kappa_1=2.0$, and $\kappa_A/\kappa_1=0.25$, $\alpha=1.2$ (left), 1.5 (middle), 1.8 (right). (Color) (B) The same as (A) but for fast fluctuations $\Omega_0\kappa_1=0.2$, and $\kappa_A\Omega_0=0.5$, $\alpha=1.2$ (left), 1.5 (middle), 1.8 (right).

$$S_{\mathrm{I}8}(\omega_3,t_2=0,-\omega_1)=-\frac{\mu^4}{\hbar^3}\,\mathrm{Im}\,\frac{\tilde{\phi}'(-i\Delta\omega_3)-\tilde{\phi}'(i\Delta\omega_1)}{\Delta\omega_1+\Delta\omega_3},$$

$$S_{\mathrm{II}8}(\omega_3,t_2=0,\omega_1)=\frac{\mu^4}{\hbar^3}\,\mathrm{Im}\,\frac{\tilde{\phi}'(-i\Delta\omega_3)-\tilde{\phi}'(-i\Delta\omega_1)}{\Delta\omega_1-\Delta\omega_3}. \tag{37}$$

The lineshapes [Eqs. (39)] diverge along the lines $\Delta\omega_3=0$ and $\Delta\omega_1=0$. The divergent peak structure is summarized in Table I. The left column corresponds to situation when $\Delta\omega_3$ is held fixed at a small but nonzero value and $\Delta\omega_1$ approaches the singular point 0. Thus we consider $\Delta\omega_1\ll\Delta\omega_3$ and $\tilde{\phi}'(i\Delta\omega_1)\gg\tilde{\phi}'(-i\Delta\omega_3)$. With the asymptotic expansion

$$\tilde{\phi}'(s)\sim\kappa_A^{\alpha-1}s^{\alpha-2}, \tag{38}$$

we get the asymptotic form of divergent $S_{\mathrm{I}}(\omega_3,-\omega_1)$, and $S_{\mathrm{II}}(\omega_3,\omega_1)$ shown in the Table I. In the right column we similarly approach the singular line at $\Delta\omega_3=0$. We have verified these analytic asymptotic results numerically [not shown, it also qualitatively agrees with Fig. 6(a)].

S_{I} and S_{II} have opposite signs, and their combination S_A is finite due to interference. The divergencies are only seen at the (1,1) and (−1,−1) peaks, and not along the entire $\omega_1=\pm1$ and $\omega_3=\pm1$ lines, since the $S_{\mathrm{I}},S_{\mathrm{II}}$ divergencies cancel. S_A is finite, but nondifferentiable along these lines.

We next examine more closely the variation along the $\Delta\omega_1=0$ axis.

$$S_{A8}(\Delta\omega_3,t_2=0,\Delta\omega_1=0)=\frac{-2\mu_{eg}^4}{\hbar^3}\frac{\mathrm{Im}\,\tilde{\phi}'(i\Delta\omega_3)}{\Delta\omega_3}.$$

The asymptotic expansion [Eq. (38)] yields the analytical peak structure at $\Delta\omega_3\approx0$.

$$S_A(\Delta\omega_3,t_2=0,\Delta\omega_1=0)\approx B\Delta\omega_3^{\alpha-3},$$
$$B=\frac{2\mu_{eg}^4}{\hbar^3}\kappa_A^{\alpha-1}\sin[\pi(2-\alpha)/2]. \tag{39}$$

The analytic structure of the (−1,−1) peaks is the same. This follows from the assumed $[\hat{\Psi}]_{ab}=[\hat{\Psi}]_{ba}$ symmetry of TSJ model, which implies $S_\nu(\omega_3+\Omega_{eg},t_2,\omega_1\mp\Omega_{eg})=S_\nu(-\omega_3+\Omega_{eg},t_2,-\omega_1\mp\Omega_{eg})$; upper sign applies for $\nu=\mathrm{I}$ lower for $\nu=\mathrm{II},A$. Based on Fig. 6(a), the peaks are more localized with steeper contours for smaller α. In all cases we see a dip at (0,0).

The two peaks induced by $\hat{G}_8$ are universal and survive even for the case of fast fluctuations $\Omega_0\kappa_1\ll1$, as shown at Fig. 6(b). Rapid changes during t_1 and t_3 induce a new peak at the average frequency (0,0) (motional narrowing). The S_A (0,0) peak is Lorentzian: The starlike contours, best seen for $\alpha=1.2$, correspond to a product of two Lorentzians along ω_1 and ω_3. The S_{I} and S_{II} lineshapes are similar. Both may be described by a statistical mixture of rapidly fluctuating particles responsible for the central peak, with the static phase responsible for the divergent peaks at the fundamental frequencies. Surprisingly, this picture is most pronounced for small $\alpha=1.2$ where all peaks are well separated. Increasing α broadens the (−1,−1) and (1,1) peaks, making them interfere with the central peak, and the Lorentzian shape becomes less pronounced as $\alpha\to2$.

The variation of S_A with t_2 in the slow fluctuation limit is displayed in Fig. 7. For t_2 longer than the mean waiting time κ_1 fractions of trajectories have different frequencies in the t_1 and t_3 intervals, as described by the G_6 contribution resulting in new cross peaks at (−1,1) and (1,−1). Since we are in the slow fluctuation limit the peaks are still well resolved. Both diagonal and cross peak contours are elongated along the $\omega_{1,3}=\pm1$ directions. Nevertheless the decay of the G_6 contribution $t_{1,3}^{\alpha-3}$ (compared to the diverging $t_{1,3}^{\alpha-2}$ decay of G_8 which is relevant for diagonal peaks) is integrable and thus the cross peaks do not diverge. Another notable point is the breakdown of Eq. (32) at $\omega_{1,3}=\pm1$. Memory loss is not com-

TABLE I. S_{I}, S_{II} lineshapes shows divergent growth along the $\omega_3=\Omega_{eg}-\Omega_0$ and $\omega_1=\Omega_{eg}-\Omega_0$ lines. Table I shows their asymptotic form.

Fixed	$\Delta\omega_3$	$\Delta\omega_1$
Varied	$\Delta\omega_1$	$\Delta\omega_3$
$S_{\mathrm{I}}(\omega_3,-\omega_1)\sim\frac{\mu^4}{\hbar^3}\sin[\pi(2-\alpha)/2]\times$	$\mathrm{sgn}(\Delta\omega_1)\frac{\lvert\Delta\omega_1\rvert^{\alpha-2}}{\Delta\omega_3}$	$-\mathrm{sgn}(\Delta\omega_3)\frac{\lvert\Delta\omega_3\rvert^{\alpha-2}}{\Delta\omega_1}$
$S_{\mathrm{II}}(\omega_3,\omega_1)\sim\frac{\mu^4}{\hbar^3}\sin[\pi(2-\alpha)/2]\times$	$-\mathrm{sgn}(\Delta\omega_1)\frac{\lvert\Delta\omega_1\rvert^{\alpha-2}}{\Delta\omega_3}$	$\mathrm{sgn}(\Delta\omega_3)\frac{\lvert\Delta\omega_3\rvert^{\alpha-2}}{\Delta\omega_1}$

plete since the algebraic functions do not factorize. At other frequencies the lineshapes approach this limiting lineshapes [Eq. (32)] algebraically as $t^{1-\alpha}$.[28] These simulations illustrate the capacity of 2DCS to probe anomalous relaxation during the t_2 interval.

V. NONSTATIONARY ENSEMBLES: AGING OF 2D LINESHAPES

In our earlier work[28] we considered nonstationary ensembles with $0<\alpha<1$ by assuming that the random walk is started by a jump at the time origin, coinciding with the first laser pulse, so that response may be calculated by $\psi'=\psi$. The lack of microscopic reversibility is reflected in violations of the symmetry relations [Eq. (28)]. The higher mobility during the (earlier) t_1 interval compared to t_3 resulted in broader peaks along the ω_1 axis compared to ω_3.

Here we explore signatures of aging. We consider random walks, which start by a jump made at some time t_0 before the first laser pulse and examine how the nonlinear lineshapes vary with t_0. The response function then depends t_0 even for $t_0\to\infty$. This is known as aging. All aging effects are fully described by calculating the WTDF $\Psi'(t;t_0)$ for the first jump which is now t_0 dependent which must be consistent with the CTRW dynamics during the t_0 period.

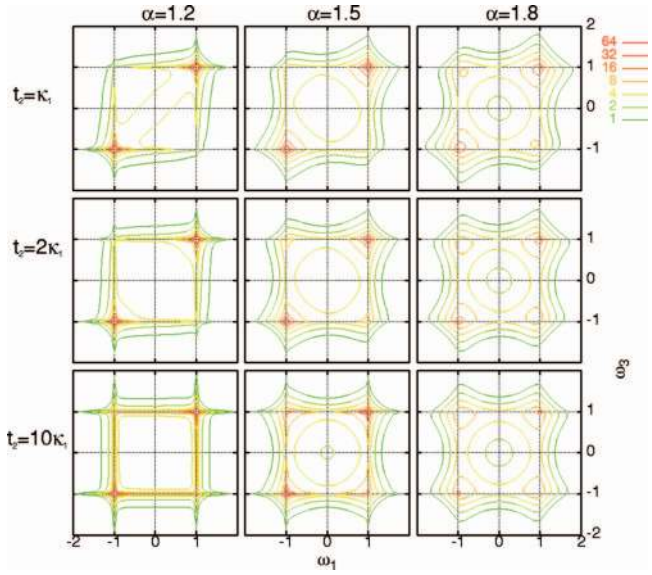

FIG. 7. (Color) The S_A signal [Eq. (15)] for the WTDF [Eq. (33)] for (left to right) $\alpha=1.2,1.5,1.8$, and $\kappa_A/\kappa_1=0.25$, $\Omega_0\kappa_1=2.0$, $t_2=\kappa_1$ (top), $t_2=2\kappa_1$ (middle), $t_2=10\kappa_1$ (bottom).

$\Psi'(t;t_0)$ can be calculated along the lines of Eq. (21) by omitting the coherence evolution $\hat{L}^{(0)}=0$ during t_0,

$$\hat{\Psi}'(t,t_0)=\hat{\Psi}(t+t_0)+\int_0^{t_0}d\xi_2\int_0^{t_0-\xi_2}d\xi_1\hat{\Psi}(t+\xi_2)\times\hat{\Sigma}(t_0-\xi_2-\xi_1)\hat{\Psi}(\xi_1).$$

In Laplace space we find for our TSJ model

$$\tilde{\psi}'(s;s_0)=\frac{[\tilde{\psi}(s_0)-\tilde{\psi}(s)]}{[1-\tilde{\psi}(s_0)](s-s_0)}. \tag{40}$$

The 2D lineshapes may thus be calculated using the algorithm presented in Sec. III. The t_0 dependence is obtained by numerically inverting these Laplace domain formulas.

The long t_0 limit may be obtained by setting $s_0\to 0$. For CTRW with finite κ_1 the denominator in Eq. (40) is

$$1-\tilde{\psi}(s_0)\approx -s_0\left.\frac{d\tilde{\psi}(s)}{ds}\right|_{s=0}=\kappa_1 s_0.$$

This reproduces the WTDF of the first jump for a stationary random walk $\psi'(t;t_0)=\phi(t)/\kappa_1$.

The lack of stationarity has some important consequences. As pointed in Ref. 50, frequency domain absorption measurement is no longer given by the Fourier transformed response function. Thus the absorption of an aging ensemble cannot be calculated using Eq. (34). Fortunately, 2DCS works in the time domain, and the measurement directly probes the response function. Thus the problems discussed in Ref. 50 do not apply for impulsive time-domain techniques such as 2DCS lineshape.

A more subtle point is that due to the lack of equilibration, the averaging over consecutive pulse sequences may depend on the experimental data acquisition repetition rate. Proper definition of the response function requires a careful preparation $\psi'(t)$ before each pulse sequence.

We have calculated the response functions, the variation of the lineshape, with the preparation time t_0 for the following model:

$$\tilde{\psi}_N(s)=\frac{1}{1+(\kappa s)^\alpha},\quad \alpha\in(0,1). \tag{41}$$

This corresponds to a WTDF with algebraic tails $\psi(t)\sim(\kappa/t)^{1+\alpha}$.

We took $\alpha=0.98$, which is close to the Markovian case [Eq. (41) for $\alpha=1$] in the fast fluctuation limit $\kappa\Omega_0\ll 1$. This

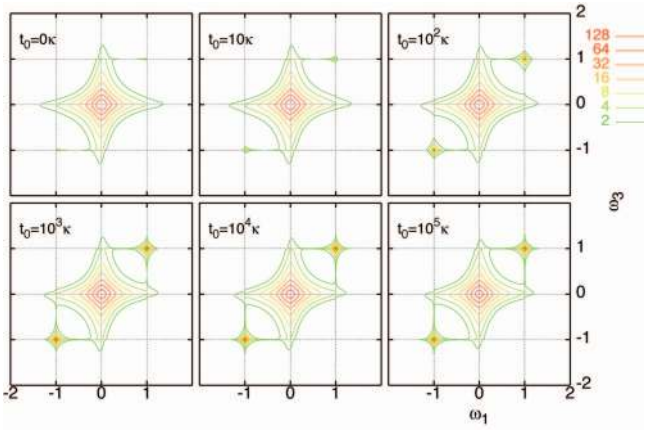

FIG. 8. (Color) Aging effects in 2D lineshapes. The S_A signal [Eq. (15)] for the nonstationary random walk model [Eq. (41)] $t_2=0$, $\kappa\Omega_0=0.2$, $\alpha=0.98$ for various initial times (from left top to right bottom) $t_0=0\kappa$, 10κ, $10^2\kappa$, $10^3\kappa$, $10^4\kappa$, $10^5\kappa$.

choice is motivated by the simpler interpretation of the lineshapes; we expect it to be closer to the Markovian case than the rather complex $t_0=0$ shapes presented in Ref. 28. The effect of t_0 could thus be better isolated. In addition, aging effects appear at arbitrarily long timescales (for suitable choice of parameters). This overcomes the difficulty with strongly anomalous ensembles, whose lineshapes cannot be obtained by repeated measurements on the same sample, whose response function is changed between two pulse sequences.

The top left panel of Fig. 8 ($t_0=0$) shows fast fluctuation Markovian contours and only tiny peaks at (1,1) and (−1, −1). No signatures of time irreversibility are seen since Eq. (28) is nearly satisfied. We next increase the aging time t_0 as we move from the top left panel to bottom right panel. The (1,1) and (−1,−1) peaks appear and grow, while the central peaks slowly get weaker. This reflects decrease of the jump rate with time. Some small deviation from the symmetry relation [Eq. (28)] can be noticed. The process is nearly reversible on the Ω_0^{-1} timescale which dominates the lineshapes. A remarkable point is that the central (motional narrowing) peak coexists with these static limit peaks. The anomalous process is better viewed as a mixture of static and fluctuating particles, rather than a homogeneous rate.

This clearly distinguishes our algorithm from calculations based on time-dependent rate master equations, which do not allow to properly describe memory effects in multipoint probes. To support this statement we have constructed Markovian process subjected to the same master equation, i.e., we require correct prediction of total densities and subsequently apply them to calculate response or multipoint correlation function based on Markovian schemes. The trajectory picture of both approaches is different.[67]

Consider a Markovian master equation whereby densities evolve in the same way as the aging random walk for arbitrary initial densities, i.e., it has same Green's function $G(t)$,

$$\rho(t) = G(t)\rho(0). \tag{42}$$

The master equation is constructed by differentiating Eq. (42) with respect to time,

$$\frac{d\rho(t)}{dt} = A(t)\rho(t), \quad A(t) \equiv \frac{dG(t)}{dt}G^{-1}(t). \tag{43}$$

The transition matrix A of time-convolutionless master equation is thus uniquely defined. Green's function [Eq. (42)] is the solution of the master equation

$$G(t) = \exp_T \int_0^t A(t')dt'. \tag{44}$$

We consider a symmetric two state dynamics parametrized by a single function Λ,

$$A(t) = \begin{pmatrix} -\Lambda(t) & \Lambda(t) \\ \Lambda(t) & -\Lambda(t) \end{pmatrix}.$$

Equation (44) can be solved after a simple algebra. This gives

$$G_{11}(t) - G_{10}(t) = \exp\left[-2\int_0^t \Lambda(t')dt'\right]. \tag{45}$$

Inverting Eq. (45), the rates can be calculated once Green's function is known

$$\Lambda(t) = \frac{-\frac{d}{dt}[G_{11}(t) - G_{10}(t)]}{2[G_{11}(t) - G_{10}(t)]}. \tag{46}$$

We next adjust Green's function to agree with those of our aging random walk. In Laplace space it reads

$$G_{11}(s) - G_{10}(s) = \frac{\phi(s)}{1+\psi(s)} = \frac{1-\psi(s)}{s[1+\psi(s)]}.$$

For the model [Eq. (41)],

$$G_{11}(s) - G_{10}(s) = \frac{(\kappa s)^\alpha}{s[2+(\kappa s)^\alpha]},$$

which may be also calculated directly in time domain as series

$$G_{11}(t) - G_{10}(t) = \sum_{n=0}^{\infty} (-2)^n \frac{(t/\kappa)^{\alpha n}}{\Gamma(n\alpha+1)}, \tag{47}$$

with the gamma function $\Gamma(y) \equiv \int_0^\infty x^{y-1}e^{-x}dx$. The master equation is thus defined by combining Eqs. (43), (46), and (47). The rates decay asymptotically $(t\to\infty)$ as $\Lambda(t) \approx \alpha/(2t)$. Exponential WTDF's $(\alpha=1)$ correspond to constant rate $\Lambda=\kappa^{-1}$.

Figure 9 shows the time-dependent rate of the master equation for various α. Aging effects (decreasing mobility with time) are reflected in the decreasing rates. Increasing α the decay is slower when approaching the Markovian limit $(\alpha=1)$ and the rates change slowly for long periods. This regime is particularly interesting because it may provide sufficient time to measure the rate constant by, e.g., lineshape experiments and give clear meaning to our arguments. (Diverging rates at very small times $t \ll \kappa$ are integrable and thus insignificant.)

We shall compare two types of stochastic processes subjected to the same master equation but with different unraveling into trajectories.[14] Aging lineshapes for the CTRW model were already presented at Fig. 8. The second model is

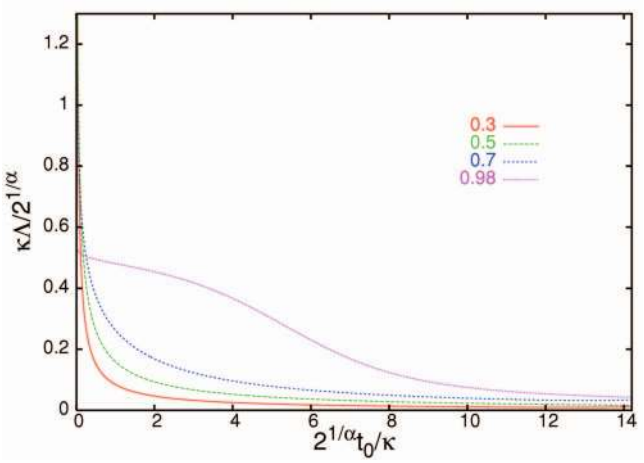

FIG. 9. (Color) Time-dependent rates of aging random walk [Eq. (46)] for $\alpha=0.3$ (solid), 0.5 (dashed), 0.7 (short-dashed), and 0.98 (dotted line).

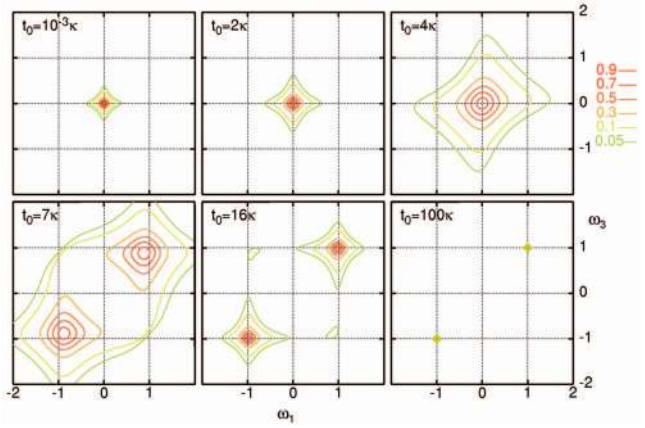

FIG. 10. (Color) Aging 2D Markovian lineshape [Eq. (48)] for various initial times $t_0=10^{-3}\kappa$, 2κ, 4κ, 7κ, 16κ, and 100κ. Master equation for probability densities corresponds to the random walk of Fig. 8.

defined by Markovian prescription: The probability of jumps is independent of the past trajectory. The stochastic Liouville equations and Green's function technique may then be used to calculate the nonlinear response.

$$R_\nu(t_3,t_2,t_1;t_0)=\theta(t_3)\theta(t_2)\theta(t_1)\times\left\langle \exp_T\left[\int_{\tau_2}^{\tau_3}[A(\tau_3')+\hat{L}^{(3)}]d\tau_3'\right]\times\exp_T\left[\int_{\tau_1}^{\tau_2}A(\tau_2')d\tau_2'\right]\times\exp_T\left[\int_{\tau_0}^{\tau_1}[A(\tau_1')\pm\hat{L}^{(1)}]d\tau_1'\right]\right\rangle.$$

We are interested in the peak pattern, which is influenced by fluctuations on the Ω_0^{-1} timescale. We consider a parameter regime where the rate does not change significantly on this timescale, and thus the peak pattern may be analyzed by a simple approximation of rates independent of t_1 and t_3 and analyze aging of $t_2=0$ lineshapes

$$R_\nu(t_3,0,t_1;t_0)=\theta(t_3)\theta(t_2)\theta(t_1)\langle\exp[(A(t_0)+\hat{L}^{(3)})t_3]\exp[(A(t_0)\pm\hat{L}^{(1)})t_1]\rangle.$$

We then obtain

$$S_\beta(\omega_3,0,\omega_1;t_0)=\frac{2\mu^4}{\hbar^3}\,\mathrm{Re}\,\frac{4\Lambda^2-\omega_3\omega_1\mp\Omega_0^2-i2\Lambda(\omega_3+\omega_1)}{[\omega_1^2-\Omega_0^2+i2\omega_1\Lambda][\omega_3^2-\Omega_0^2+i2\omega_3\Lambda]},\tag{48}$$

where the upper (lower) sign is for $\beta=$I ($\beta=$II) and where $\Lambda\equiv\Lambda(t_0)$.

The aging Markovian 2D absorptive lineshapes are presented at Fig. 10. The central peak is gradually broadened with increasing time (and decreasing rates) and splits into two peaks centered along diagonal at fundamental frequency. These peaks get narrower for long t_2.

The significance of the different trajectory picture can be seen by comparing the two lineshapes at Figs. 8 and 10. We notice that the crossover to static lineshapes is somewhat faster at Fig. 10. This is, however, less obvious feature, since it depends on chosen particular parametrization. The more significant feature, which distinguishes the two models, is that the static peaks at fundamental frequencies and the fast motional narrowing central peak never coexist at Fig. 10 in contrast to Fig. 8.

This may be explained as the direct signature of memory. The CTRW model shows two populations: static and fast fluctuating, i.e., particles are differentiated based on their histories. In contrast all particles in the Markovian model have homogenous probabilities for the next jump. This lack of memory is reflected in the unique peak pattern with no simultaneous static and fast fluctuating signatures in the spectrum.

These two models are nonequivalent since they assign different trajectory pictures to the same density matrix, as is clearly seen from the higher order correlation functions and response. The coexistence of both static and fast fluctuations in spectra clearly reflects the additional information, beyond the two point correlation functions.

The unraveling of master equations into trajectories is an important issue. Two-dimensional lineshapes which are sensitive to the trajectories should provide a direct test for the unraveling schemes.[14] Single molecule spectroscopy looks at the trajectories one at a time. Multidimensional spectroscopy looks at the entire ensemble but unravels it by the manipulation of coherence.

In summary, our simulations demonstrate that two-dimensional correlation plots of signals obtained from the response of the system to sequences of multiple laser pulses carry specific and direct signatures of complex dynamics. Such techniques are currently feasible in many spectral regimes, NMR, EPR, the infrared (vibrations, phonons), and in the visible (electronic excitations).

ACKNOWLEDGMENTS

The support of the Ministry of Education, Youth and Sports of the Czech Republic (Project No. MSM 0021620835), GAČR (Grant No. 202/07/P245) (F.Š.), NSF

(Grant No. CHE-0446555) and NIH (GM59230) (S.M.) is gratefully acknowledged.

[1] H. Yang, G. Luo, P. Karnchanaphanurach, T.-M. Louie, I. Rech, S. Cova, L. Xun, and X. S. Xie, Science **302**, 262 (2003).
[2] F. Amblard, A. C. Maggs, B. Yurke, A. N. Pargellis, and S. Leibler, Phys. Rev. Lett. **77**, 4470 (1996).
[3] R. Verberk and M. Orrit, J. Chem. Phys. **119**, 2214 (2003).
[4] M. Kuno, D. P. Fromm, S. T. Johnson, A. Gallagher, and D. J. Nesbitt, Phys. Rev. B **67**, 125304 (2003).
[5] K. T. Shimizu, R. G. Neuhauser, C. A. Leatherdale, S. A. Empedocles, W. K. Woo, and M. G. Bawendi, Phys. Rev. B **63**, 205316 (2001).
[6] O. Flomenbom, K. Velonia, D. Loos, S. Masuo, M. Cotlet, Y. Engelborghs, J. Hofkens, A. E. Rowan, R. J. M. Nolte, M. Van der Auweraer, F. C. De Schryver, and J. Klafter, Proc. Natl. Acad. Sci. U.S.A. **102**, 2368 (2005).
[7] J. Sabelko, J. Ervin, and M. Gruebele, Proc. Natl. Acad. Sci. U.S.A. **96**, 6031 (1999).
[8] M. Oliveberg and P. G. Wolynes, Q. Rev. Biophys. **38**, 245 (2005).
[9] R. Metzler and J. Klafter, J. Phys. A **37**, R161 (2004).
[10] J. W. Kirchner, X. Feng, and C. Neal, Nature (London) **403**, 524 (2000).
[11] I. E. T. Iben, D. Braunstein, W. Doster, H. Frauenfelder, M. K. Hong, J. B. Johnson, S. Luck, P. Ormos, A. Schulte, P. J. Steinbach, A. H. Xie, and R. D. Young, Phys. Rev. Lett. **62**, 1916 (1989).
[12] R. H. Austin, K. Beeson, L. Eisenstein, H. Frauenfelder, I. C. Gunsalus, and V. P. Marshall, Phys. Rev. Lett. **32**, 403 (1974).
[13] F. Mainardi, M. Raberto, R. Gorenflo, and E. Scalas, Physica A **287**, 468 (2000).
[14] H.-P. Breuer and F. Petruccione, *The Theory of Open Quantum Systems* (Oxford University Press, Oxford, 2002).
[15] H. Frauenfelder, S. G. Sligar, and P. G. Wolynes, Science **254**, 1598 (1991).
[16] V. Lubchenko and P. G. Wolynes, Annu. Rev. Phys. Chem. **58**, 235 (2007).
[17] R. Granek and J. Klafter, Phys. Rev. Lett. **95**, 098106 (2005).
[18] R. Zwanzig, Lect. Theor. Phys. **3**, 106 (1960).
[19] R. Metzler and J. Klafter, Phys. Rep. **339**, 1 (2000).
[20] V. M. Kenkre, E. W. Montroll, and M. F. Shlesinger, J. Stat. Phys. **9**, 45 (1973).
[21] P. Allegrini, G. Aquino, P. Grigolini, L. Palatella, A. Rosa, and B. J. West, Phys. Rev. E **71**, 066109 (2005).
[22] F. Šanda and S. Mukamel, Phys. Rev. E **72**, 031108 (2005).
[23] R. F. Fox, Phys. Rep. **48**, 179 (1978).
[24] A. O. Caldeira and A. J. Leggett, Physica A **121**, 587 (1983).
[25] S. C. Kou and X. S. Xie, Phys. Rev. Lett. **93**, 180603 (2004).
[26] W. E. Montroll and G. H. Weiss, J. Math. Phys. **6**, 167 (1965).
[27] G. H. Weiss, *Aspects and Applications of the Random Walks* (North-Holland, Amsterdam, 1994).
[28] F. Šanda and S. Mukamel, Phys. Rev. Lett. **98**, 080603 (2007).
[29] J. Klafter, M. F. Shlesinger, and G. Zumofen, Phys. Today **49**, 33 (1996).
[30] M. F. Shlesinger, J. Stat. Phys. **10**, 421 (1974).
[31] M. F. Shlesinger, Annu. Rev. Phys. Chem. **39**, 269 (1988).
[32] J. P. Bouchard and A. Georges, Phys. Rep. **195**, 127 (1990).
[33] G. Bel and E. Barkai, Phys. Rev. Lett. **94**, 240602 (2005).
[34] G. Margolin and E. Barkai, Phys. Rev. Lett. **94**, 080601 (2005).
[35] X. Brokmann, J. P. Hermier, G. Messin, P. Desbiolles, J.-P. Bouchaud, and M. Dahan, Phys. Rev. Lett. **90**, 120601 (2003).
[36] E. Sparre Andersen, Math. Scand. **1**, 263 (1953).
[37] E. Sparre Andersen, Math. Scand. **2**, 295 (1954).
[38] S. Redner, *A Guide to First-Passage Processes* (Cambridge University Press, Cambridge, 2001).
[39] D. M. Jonas, Annu. Rev. Phys. Chem. **54**, 425 (2003).
[40] S. Mukamel, Annu. Rev. Phys. Chem. **51**, 691 (2000).
[41] Y. Tanimura and S. Mukamel, J. Chem. Phys. **99**, 9496 (1993).
[42] R. R. Ernst, G. Bodenhausen, and A. Wokaun, *Principles of Nuclear Magnetic Resonance in One and Two Dimensions* (Oxford University Press, New York, 1987).
[43] J. Wang, J. Chen, and R. M. Hochstrasser, J. Phys. Chem. B **110**, 7545 (2006).
[44] J. Zheng, K. Kwak, J. Asbury, X. Chen, I. R. Piletic, and M. D. Fayer, Science **309**, 1338 (2005).
[45] Y. S. Kim and R. M. Hochstrasser, Proc. Natl. Acad. Sci. U.S.A. **102**, 1185 (2005).
[46] T. Brixner, J. Stenger, H. M. Vaswani, M. Cho, R. E. Blankenship, and G. R. Fleming, Nature (London) **434**, 625 (2005).
[47] Y. Tanimura, J. Phys. Soc. Jpn. **75**, 082001 (2006).
[48] P. W. Anderson, B. I. Halperin, and C. M. Varma, Philos. Mag. **25**, 1 (1971).
[49] R. Kubo, J. Math. Phys. **4**, 174 (1963).
[50] Y. Jung, E. Barkai, and R. Silbey, Chem. Phys. **284**, 181 (2002).
[51] A. I. Shushin, Phys. Rev. E **64**, 051108 (2001).
[52] H. Qian and H. Wang, Europhys. Lett. **76**, 15 (2006).
[53] This condition is satisfied for any TSJ random walk (even asymmetric $[\Psi]_{ab} \neq [\Psi]_{ba}$). Further important class of such random walks are separable WTDF $[\Psi]_{ji}=T_{ji}\psi(t)$, provided that T is detail balanced.
[54] J. Schnakenberg, Rev. Mod. Phys. **48**, 571 (1976).
[55] G. Aquino, L. Palatella, and P. Grigolini, Phys. Rev. Lett. **93**, 050601 (2004).
[56] F. Barbi, M. Bologna, and P. Grigolini, Phys. Rev. Lett. **95**, 220601 (2005).
[57] N. G. van Kampen, *Stochastic Processes in Physics and Chemistry* (North-Holland, Amsterdam, 1992).
[58] S. Mukamel, *Principles of Nonlinear Optical Spectroscopy* (Oxford University Press, New York, 1995).
[59] Ch. Scheurer and S. Mukamel, J. Chem. Phys. **115**, 4989 (2001).
[60] M. Khalil, N. Demirdöven, and A. Tokmakoff, Phys. Rev. Lett. **90**, 047401 (2003).
[61] F. Šanda and S. Mukamel, J. Chem. Phys. **125**, 014507 (2006).
[62] T. l. C. Jansen, W. Zhuang, and S. Mukamel, J. Chem. Phys. **121**, 10577 (2004).
[63] T. l. C. Jansen, T. Hayashi, W. Zhuang, and S. Mukamel, J. Chem. Phys. **123**, 114504 (2005).
[64] F. Šanda and S. Mukamel, Phys. Rev. E **73**, 011103 (2006).
[65] A. I. Shushin, Phys. Rev. E **67**, 061107 (2003).
[66] When the system's evolution (and equilibrium) depends on a state of chromophore, which goes beyond the present stochastic model, there will be time directionality of contributions evolving in *ee* state during t_2 R_i, R_{iii}. Equation (28) is thus broken. For the same reasons in the long t_2 limit Eqs. (29) and (30) are modified to $R_{iii}(t_3,t_2,t_1)=(i/\hbar)K_e(t_3)K(t_1)$ and $R_{iv}(t_3,t_2,t_1)=K_e(t_3)K^*(t_1)$, where K_e represents linear response of the excited state equilibrium at the beginning of t_3 interval. Eq. (32) should be then replaced by $\hbar S_A(\omega_3,t_2\rightarrow\infty,\omega_1)=2W_A(\omega_1)[W_A(\omega_3)+W_E(\omega_3)]$. where $W_E(\omega)\equiv \mathrm{Re}\int_0^\infty K_e(t)\exp[i(\omega-\Omega_{eg})t]dt$ is the emission lineshape.
[67] P. Allegrini, F. Barbi, P. Grigolini, and P. Paradisi, Phys. Rev. E **73**, 046136 (2006).